Simulation of Updraft and Downdraft Gasification Using Computational Fluid Dynamics (CFD) for Production of Hydrogen-Rich Syngas from Cow Manure Waste

Manuscript received September 21, 2025; revised December 26, 2025

Amaliyah Rohsari Indah Utami
Engineering Physics
Universitas Telkom
Bandung, Indonesia
https://orcid.org/0000-0002-3077-2285

Anindya Nabila Salma
Engineering Physics
Universitas Telkom
Bandung, Indonesia
anindyans99@gmail.com

Daffa Rayhan Betha Muchtar
Engineering Physics
Universitas Telkom
Bandung, Indonesia
daffa.ryhn@gmail.com

Neni Sintawardani
National Research and Innovation Agency (BRIN)
Bandung, Indonesia
https://orcid.org/0000-0001-8657-1311

Suwandi
Engineering Physics
Universitas Telkom
Bandung, Indonesia
suwandi@telkomuniversity.ac.id

***Abstract*- Biomass gasification offers a promising route to low-carbon hydrogen, yet the operating conditions and reactor configuration governing hydrogen-rich syngas remain insufficiently compared across practical regimes. This study aims to quantify the effects of gasifier type (updraft vs. downdraft), operating temperature, and superficial velocity on hydrogen production performance, with emphasis on the syngas H_2/CO ratio. Computational fluid dynamics simulations were implemented to model devolatilization, oxidation, and reduction pathways under steady-state assumptions, while systematically varying temperature (680-800°C) and air superficial velocity (0.0025-4 m/s). Model validation against experimental reference data demonstrated good agreement, with relative errors ranging from 5.95% to 6.93%. The results indicate that a downdraft configuration operated at 680°C and 2 m/s maximizes the H_2/CO ratio, achieving a value of 2.091, outperforming alternative settings in terms of hydrogen yield and energy efficiency, albeit with higher variability than the updraft configuration. Increasing air flow beyond this optimum diminishes the H_2/CO ratio due to enhanced oxidation, whereas raising the temperature to 800°C generally reduces the average H_2/CO across both configurations. These findings establish a practical operating window for hydrogen-rich syngas from livestock waste and highlight the need for rigorous process control to manage variability in downdraft operation. The study provides evidence-based guidance for gasifier design and operation, aiming to achieve efficient and renewable hydrogen production.**

Keywords—CFD Simulation, Downdraft Gasification, H_2/CO Ratio, Process Optimization, Updraft Gasification

I. INTRODUCTION

Global population growth is driving sustained increases in energy demand, while fossil energy reserves and their environmental viability continue to diminish, underscoring the need to accelerate the deployment of reliable and scalable renewable energy systems [1–3]. This context highlights the need to accelerate the deployment of renewable energy systems as scalable and dependable substitutes [2, 3]. Among renewable options, biomass is particularly promising due to its availability and potential for a circular economy, including the valorization of livestock waste, such as cattle manure [3, 4].

At the same time, growing populations drive higher demand for animal protein, which consequently increases livestock manure generation such as cattle manure [5–7]. Given its readily degradable organic fraction, cattle manure biomass is a viable feedstock for syngas production via gasification [8–11].

An effective and efficient pathway for cattle manure management is thermochemical conversion via gasification, which enables simultaneous waste mitigation and energy recovery [12–15]. Gasification converts solid carbonaceous feedstocks into synthesis gas (syngas), which is composed primarily of H_2, CO, CO_2, and CH_4, supporting diverse end uses, including power generation, hydrogen production, and liquid fuel synthesis through subsequent conditioning and upgrading steps [14, 16, 17].

Gasification proceeds through four canonical zones-drying, pyrolysis, combustion, and reduction-each governing the removal of moisture, the release of volatiles, partial oxidation, and char-gas reactions that ultimately determine the syngas composition [18, 19]. Two fixed-bed configurations are commonly employed: updraft and downdraft, with distinct thermo-fluid characteristics and tar-formation behaviors. In practice, updraft systems often exhibit higher apparent conversion efficiency due to counter-current heat recovery, whereas downdraft systems typically suppress tar carryover through a high-temperature reaction throat, producing cleaner syngas for downstream utilization.

Comparative evaluations that explicitly link cattle-manure gasification to hydrogen-rich syngas formation across updraft and downdraft reactors using engineering-grade ANSYS CFD workflows are sparse, leaving practical operating guidance underdeveloped. Accordingly, this study employs Computational Fluid Dynamics in ANSYS to simulate manure-derived biomass conversion in both configurations, quantifying how operating temperature and air superficial velocity shape the H_2/CO ratio and related performance metrics [20–22], and comparing reactor-specific

 ISSN: 2961-872X ●PISSN: 2961-8924 ●DOI: 10.56741/IISTR.esl.001397

characteristics and efficiencies to identify an optimal operating window for hydrogen production.

II. Materials and Methods

A. Material

Materials used in this simulation consist of cattle manure waste. The cattle manure waste was characterized using ultimate and proximate analyses. These analyses include parameters such as carbon, hydrogen, nitrogen, and oxygen contents (ultimate analysis), as well as moisture, volatile matter, fixed carbon, and ash contents (proximate analysis). In this study, syngas compositions are reported on a dry, N_2-free basis, and the mole fractions of CO, H_2, CH_4, and CO_2 are renormalized such that they sum to unity for each operating condition. The results of these analyses are presented in Table I.

Table I. Results of ultimate and proximate analysis of cow manure waste (air-dried) [23]

Proximate Contents (wt.%)	
Moisture (wt %)	6.2
Ash (wt %)	33.3
Volatile Matter (wt %)	50.8
Fixed Carbon (wt %)	15.8
Bulk Density (kg/m^3)	300
Ultimate analysis (dry and ash free basis) (wt.%)	
Hydrogen (wt %)	5.9
Carbon (wt %)	47.5
Nitrogen (wt %)	4.1
Oxygen (wt %)	42.5

Ultimate analysis values are given on a dry, ash-free basis, resulting in totals that are less than 100% when compared with proximate analysis (which is performed on air-dried samples and includes ash and moisture). This is a standard practice to characterize organic and inorganic fractions in biomass feedstock analysis separately. In this study, syngas compositions are reported on a dry, N_2-free basis, and the mole fractions of CO, H_2, CH_4, and CO_2 are renormalized such that they sum to unity for each operating condition.

B. Gasification Reactor Dimension Design

The dimensions of the gasification reactor were determined using empirical design relations that link the feedstock consumption rate and specific gasification rate to the required cross-sectional area and bed height. In this work, the feedstock consumption rate (FCR) is set to 1 kg/h, consistent with the mass-flow assumptions used in the Computational Fluid Dynamics (CFD) model within ANSYS software [23–26]. Various process parameters influencing the design [27–29] are shown in Table II.

Table II. Gasification reactor dimension parameters [28,30,31]

Parameter	Units
Mass flow rate of input	1 kg/h
Specific Gasification Ratio (SGR)	100 kg/m^2
Reaction time of gasification (t_c)	14 h
Temperature (T)	680°C
Density of cattle manure waste (ρ_c)	411.2 kg/m^3
Equivalence Ratio (ER)	0.15
Air density (ρ_a)	1.25 kg/m^3
Air superficial velocity (V_a)	0.0025 m/s
Stoichiometric Air-Fuel Ratio (SA)	5.3

In this study, the global equivalence ratio (ER) is fixed at 0.15 by prescribing a constant cattle-manure feed rate of 1 kg/h and determining the corresponding stoichiometric air requirement from the ultimate analysis and the stoichiometric air-fuel ratio (SA = 5.3 kg air/kg fuel). The actual air mass flow rate for each case is then set to 0.15 times the stoichiometric demand, so that the global ER remains 0.15 for all simulations. The imposed superficial air velocities of 0.0025, 1, 2, and 4 m/s are obtained by adjusting the effective inlet cross-sectional area in the CFD geometry while keeping the air mass flow rate consistent with ER = 0.15, which ensures that changes in superficial air velocity primarily affect local flow patterns and gas residence time rather than the overall mass stoichiometry.

The reactor diameter (D) and effective bed height (H) are then calculated using equations below (30,31):

$$A = \frac{FCR}{SGR} \tag{1}$$

$$D = \sqrt{\frac{4A}{\pi}} \tag{2}$$

$$H = \frac{SGR \times t}{\rho_c} \tag{3}$$

where A is the reactor cross-sectional area (m^2), FCR is the feedstock consumption rate (kg/h), SGR is the specific gasification rate (kg/(m^2.h)), t_c is the characteristic gasification time (h), and ρ_c is the bulk density of the cattle-manure bed (kg/m^3). A unit check confirms that A has units of m² and that D and H are in meters, since

$$A = \frac{FCR}{SGR} = \frac{(\frac{kg}{h})}{(\frac{kg}{(m^2.h)})} = m^2$$

and,

$$H = \frac{SGR \times t_c}{\rho_c} = \frac{(\frac{kg}{(m^2.h)})xh}{\frac{kg}{m^3}} = m$$

The air superficial velocity (V_a) is defined as the air flow superficial velocity injected into the gasification reactor using equation (3) below [32,33]:

$$V_a = \frac{4 \times AFR}{\pi D^2} \tag{4}$$

where AFR is defined by equation (4):

$$AFR = \frac{\varepsilon \times FCR \times SA}{\rho_a} \tag{5}$$

Using the design parameters in Table II, the calculated diameter and height for the updraft reactor are D = 0.30 ± 0.01 m and H = 0.40 ± 0.02 m. In comparison, the downdraft reactor has a diameter of D = 0.165 ± 0.005 m and a height of H = 0.60 ± 0.02 m, where the uncertainties reflect plausible variations in SGR and bulk density (±5%) as well as rounding errors in empirical correlations. These dimensions are consistent with typical laboratory-scale biomass gasifiers reported in the literature, where diameters in the range of 0.16-0.30 m and heights of around 0.40-0.70 m are used for similar feed rates and moisture contents.

The chosen D and H also yield gas residence times that are compatible with the kinetic model employed in this study. For the lowest air superficial velocity (0.0025 m/s), the estimated superficial gas residence time spans several tens of seconds,

 ISSN: 2961-872X ● PISSN: 2961-8924 ● DOI: 10.56741/IISTR.esl.001397

allowing sufficient time for drying, devolatilization, oxidation, and reduction reactions to approach quasi-steady conditions, whereas at the highest air superficial velocity (4 m/s) the residence time shortens to the order of one second, consistent with the observed decrease in H_2/CO ratio due to stronger oxidation and incomplete reduction. This ordering (longer residence time at low superficial velocity and shorter at high air superficial velocity) aligns with the trends in syngas composition and H_2/CO ratio discussed in Section III, confirming that the selected reactor dimensions and operating velocities are physically consistent with the reaction kinetics and transport processes represented in the CFD model.

C. Simulation Design

The simulation design is based on the following assumptions [34–40]: a) The system operates under steady-state conditions; b) Tar formation is neglected. Tar formation and subsequent secondary reactions are neglected due to the high operating temperatures (680-800°C) and the presence of a high-temperature oxidation zone, particularly in the downdraft configuration. Under these conditions, primary tar is largely cracked before exiting the main reaction region. While this simplification is pragmatic for engineering-scale CFD, omitting tar chemistry could potentially underestimate CO_2 and H_2 yields slightly, as some carbon in heavy tar precursors would otherwise participate in gasification reactions.

However, the impact on the H_2/CO ratio is expected to be modest because tar precursors are predominantly hydrogen-depleted compounds; c) NO_x and SO_x are not produced. Nitrogen and sulfur oxide formation is neglected because the equivalence ratio (ER = 0.15) maintains a fuel-rich regime in most reactor zones, limiting the formation of thermal NO_x. For biomass feedstocks such as cattle manure with moderate nitrogen content (4.1 wt.% ultimate analysis, dry ash-free basis), the omission of NO_x/SO_x chemistry does not significantly bias syngas composition predictions under these sub-stoichiometric conditions, though it may slightly overestimate H_2 by ignoring minor oxidation pathways. For H_2/CO ratio optimization and comparative evaluation across temperatures and reactors, this neglect is acceptable; d) Non-ideal gas behavior. All gases are assumed to behave as ideal throughout the reactor, which is reasonable at moderate temperatures and pressures (atmospheric conditions, 680-800°C). Real gas corrections would add negligible (<1%) changes to density and enthalpy at these conditions and would not alter the relative ranking of operating performance; e) Volatile products consist only of H_2, CO, CO_2, CH_4, and H_2O, heavier hydrocarbons and tars are neglected (as noted above); f) The char stream consists only of solid carbon and ash, simplifying the solid-phase description. These assumptions are consistent with global pyrolysis and combustion models used in engineering practice and allow focus on the primary syngas constituents most relevant to hydrogen production and downstream processes; g) Heat losses. Heat loss from the gasifier walls is considered negligible in the steady-state CFD model.

This assumption streamlines the simulation by eliminating external boundary-layer heat transfer, focusing the analysis on in-bed reaction kinetics and thermodynamics. In reality, some wall heat loss occurs, which would lower absolute temperatures and slightly reduce the production rates of H_2 and CO. However, because the same percentage of heat loss would apply to all simulated cases, the comparative trends in H_2/CO ratio between the 680°C and 800°C cases and between updraft and downdraft configurations would be preserved. The impact on process stability and reactor-type comparison is therefore expected to be qualitatively minimal; h) The input mass flow rate of cattle manure waste is 1 kg/h.

The following boundary conditions are applied to simulate realistic operational scenarios [31)]:

a) Inlet conditions. The air superficial velocity (V_a) is varied at four levels: 0.0025 m/s, 1 m/s, 2 m/s, and 4 m/s. This range enables assessment of how different air velocities affect gasification performance. At the air inlet, a uniform superficial velocity boundary condition is applied with magnitudes of 0.0025, 1, 2, and 4 m/s, combined with a fixed inlet temperature and species mass fractions corresponding to dry air; the total air mass flow rate is constrained so that the resulting global ER is 0.15 in all cases, consistent with the stoichiometric air-fuel ratio derived from the ultimate analysis. The solid cattle-manure bed is represented through volumetric source terms for devolatilization, char reactions, and heat release, calibrated to a constant fuel feed rate of 1 kg/h. At the same time, the outlet is modeled as a pressure outlet at atmospheric pressure, allowing the syngas mass flow and composition to adjust according to the internal solution. Under these conditions, increasing the nominal air superficial velocity at a fixed ER corresponds physically to changing the effective inlet area, thereby modifying the local flow field and residence time distribution without altering the global mass and energy balance between fuel and oxidizer. The imposed air velocities, ranging from 0.0025 to 4 m/s, span laminar to weakly transitional flow regimes within the packed-bed reactors, resulting in significant variations in Reynolds number and gas residence time. A Reynolds-number estimate based on the bed diameter and gas properties confirms that the flow remains within a range where the adopted pressure-based segregated solver and turbulence treatment are appropriate, with turbulence effects confined mainly to the vicinity of the air inlets and, for the downdraft unit, the throat region. In contrast, the bulk of the bed behaves predominantly as laminar or weakly transitional flow.

b) Temperature. The reactor operates at 680°C and 800°C. These temperatures are critical for evaluating the thermal efficiency of the gasification process. For each operating point, the inlet mass balance is satisfied.

$$\dot{m}_{fuel} + \dot{m}_{air} = \dot{m}_{syngas} + \dot{m}_{ash} \tag{6}$$

with

$$\dot{m}_{fuel} = 1\ \frac{kg}{h} \tag{7}$$

$$\dot{m}_{air} = \mathrm{ER} \times \mathrm{SA} \times \dot{m}_{fuel} = 0.15 \times 5.3 \times 1 \frac{kg}{h}$$

and $\dot{m}_{ash}$ determined from the proximate analysis of the ash fraction. The energy balance at the inlet includes the sensible enthalpy of the preheated air, the sensible and chemical enthalpies of the incoming fuel, and the heat of reaction released or absorbed by the global kinetic scheme. In contrast, at the outlet, it includes the sensible and chemical enthalpy of the syngas stream and the sensible enthalpy of the solid residue. Because ER, fuel feed rate, and inlet temperature are fixed for a given temperature level (680°C or 800°C), the total mass and energy input are constant across the superficial velocity cases, and differences in outlet composition and temperature are primarily governed by changes in hydrodynamics and residence time rather than changes in overall stoichiometry.

TABLE III. OPERATING CASES, GLOBAL ER, AND ESTIMATED GAS RESIDENCE TIME

Case	Gasifier type	Air superficial velocity (m/s)	Global ER (-)	Estimated gas residence time (s)
1	Updraft / Downdraft	0.0025	0.15	τ_1 (longest, low-superficial velocity regime)
2	Updraft / Downdraft	1.0	0.15	$\tau_2 < \tau_1$
3	Updraft / Downdraft	2.0	0.15	$\tau_3 < \tau_2$
4	Updraft / Downdraft	4.0	0.15	τ_4 (shortest, high-superficial velocity regime)

Table III shows that the global ER is identical (0.15) by construction for all four superficial velocity cases. In contrast, the estimated superficial gas residence time decreases monotonically as the imposed superficial velocity increases, reflecting the trade-off between reaction time and convective transport inside the reactor. The qualitative ordering $\tau_1 > \tau_2 > \tau_3 > \tau_4$ is used to interpret changes in syngas composition and H_2/CO ratio as functions of both temperature and hydrodynamic regime.

The gasification process is modeled using a combination of homogeneous (gas-phase) and heterogeneous (solid-gas) reaction kinetics that together represent the primary conversion steps of cattle-manure biomass in fixed-bed reactors. The reaction scheme explicitly includes drying, devolatilization (pyrolysis), oxidation, and reduction reactions, as summarized in Table 4, and is implemented as a set of global Arrhenius-type rate expressions, following engineering-grade biomass gasification practice. Drying and pyrolysis are described by a devolatilization law, in which the moist feedstock first releases moisture to form a dry solid, and the dry solid then decomposes into char and a volatile mixture of H_2, CO, CO_2, CH4, and H_2O, which are further consumed by homogeneous reactions as outlined in Table IV.

TABLE IV. MAIN REACTIONS IN GASIFICATION [28,41]

Main reactions in the biomass gasification process	
Drying	Moist feedstock + heat dry feedstock + H_2O
Pyrolysis (devolatilization)	Dry feedstock + heat char + volatiles
Oxydation reaction	$C + O_2 \rightarrow CO_2$ (-406 kJ/mol)
	$2H_2 + O \rightarrow 2H_2O$ (-242 kJ/mol)
Reduction reaction	$C + CO_2 \rightarrow 2CO$ (+ 172.6 kJ/mol)
Steam gasification	$C + H_2O \rightleftharpoons CO + H_2$ (+ 131.4 kJ/mol)
Methane gasification	$C + 2H_2 \rightleftharpoons CH_4$ (- 75 kJ/mol)
Water-gas shift (WGS)	$CO + H_2O \rightleftharpoons CO_2 + H_2$ (-42.3 kJ/mol)
	$CH_4 + H_2O \rightleftharpoons 4CO + 3H_2$ (+ 206 kJ/mol)

For homogeneous gas-phase kinetics, CO, H_2, CH_4, and CO_2 participate in oxidation, steam reforming, and water-gas shift (WGS) reactions, while heterogeneous kinetics describe char oxidation and char-CO_2-CO_2/H_2O gasification at the particle surface. In this study, the global reaction rates and kinetic parameters (pre-exponential factors and activation energies) are taken from biomass gasification correlations reported in the literature for similar fixed-bed systems and embedded in the CFD solver as source terms in the species and energy equations, so that the local reaction rate depends on temperature and species concentrations. Turbulence-chemistry interaction is treated in a steady-state framework: the flow field is resolved with the selected turbulence model, and the global reaction rates are evaluated directly from the mean fields rather than using additional flamelet or PDF models, which is appropriate for the moderate Reynolds numbers and predominantly laminar-transitional conditions in the packed bed.

Diffusion and mixing effects are captured through the species transport equations, which incorporate effective diffusivities that combine molecular diffusion and, where turbulence is present, turbulent diffusion. This ensures that both convective and diffusive transport contribute to the local reaction environment. This coupling enables the model to elucidate how variations in air superficial velocity and temperature influence residence time, mixing, and reaction progress, which in turn determine the syngas composition and H_2/CO ratio, as reported in Tables V and VI. The resulting reaction-transport framework provides sufficient chemical fidelity to compare updraft and downdraft configurations and assess the influence of operating conditions on hydrogen-rich syngas formation, while remaining computationally tractable for the complete set of CFD simulations.

The range of imposed superficial air velocities from 0.0025 to 4 m/s corresponds to laminar to weakly transitional flow regimes within the packed-bed region of both gasifiers. A Reynolds-number estimate based on the bed diameter and gas properties at operating temperatures shows that for the lowest superficial velocity, the flow is clearly laminar. In contrast, for the highest superficial velocity, local Reynolds numbers increase but remain within a range where a steady pressure-based segregated solver with the selected turbulence model provides a suitable representation of the flow field. Turbulence effects are therefore expected to be most relevant near the air inlets and, for the downdraft reactor, in the throat region. In contrast, the bulk of the bed behaves predominantly as a laminar or weakly transitional flow, which is consistent with the modeling assumptions used in this study.

D. Simulation Data Validation

Simulation data validation is performed to ensure that the results of the Computational Fluid Dynamics (CFD) simulations are consistent with available experimental data [31]. This process aims to assess the accuracy of the simulation model in representing actual physical phenomena and to increase confidence in the resulting simulations.

In this study, the lower heating value (LHV) of syngas is calculated on a dry, N_2-free basis, consistent with the composition reporting convention used throughout the manuscript. The input mole fractions of CO, H_2, and CH_4 in the LHV expression are therefore the renormalized dry mole fractions listed in Tables V and VI, where N_2 and H_2O are excluded from the normalization and do not contribute directly to the calorific value. The resulting LHV values are expressed in units of MJ/Nm³, where the reference state corresponds to standard conditions for gas volume measurement.

Uncertainty in the predicted LHV arises primarily from uncertainty in the simulated syngas composition, which is characterized by average species errors of approximately 6% from the validation study. Assuming this composition uncertainty propagates linearly into the LHV calculation, the LHV predictions are reported with one decimal place, and error bars of ±6% are applied in the corresponding figures to represent the combined effect of composition uncertainty on the calculated energy content of the syngas. This choice of significant figures and uncertainty bounds ensures consistency between the precision of the LHV values and the reliability of the underlying species predictions, allowing readers to interpret differences between operating conditions in light of the model's validated accuracy.

The simulations are conducted using CFD software with a focus on the thermodynamic and kinetic aspects of gasification. The mathematical model includes equations to

 ISSN: 2961-872X ● PISSN: 2961-8924 ● DOI: 10.56741/IISTR.esl.001397

calculate efficiency and the low heating value (LHV) of synthesis gas (syngas) [19]. The LHV of syngas is calculated from the dry, N_2-free mole fractions and using equation (8) below:

$$\mathrm{LHV}_{syngas} = \frac{(12.622\times \mathrm{CO})+(10.788\times H_2)+(35.814\times CH_4)}{100}\ \mathrm{Mj/Nm^3} \quad (8)$$

To assess the reliability of the simulation results, an error calculation is performed to determine the difference between the simulation data and the experimental data. The percentage error can be calculated using equation (9) below:

$$Error\ (\%): \frac{(approximate-exact)}{exact} x100(\%) \quad (9)$$

Data validation is performed by comparing the simulation results with previous studies (31). Validation is conducted at a temperature of 680°C with an air superficial velocity of 0.018 m/s. Acceptable engineering standards for error in Computational Fluid Dynamics (CFD) simulations are 10% and 25%. These threshold choices are aligned with industry standards, ensuring that the simulation results are robust and suitable for application [42–45].

To ensure the numerical robustness of the CFD predictions, a verification study was conducted in addition to the validation against experimental data. The simulations were performed using a pressure-based segregated solver under steady-state conditions, with second-order spatial discretization for the momentum, energy, and species transport equations. Convergence was monitored using scaled residuals and integral output quantities: all simulations were iterated until residuals for continuity, momentum, energy, and species fell below 10^{-4}, while key monitors (total syngas mass flow and outlet H_2 and CO mole fractions) had stabilized and exhibited no visible drift over at least 500 additional iterations.

A mesh-refinement (grid-independence) study was conducted using three systematically refined unstructured meshes for each reactor configuration. The coarse, medium, and fine grids contained approximately 1.2×10^5, 2.4×10^5, and 4.8×10^5 control volumes, respectively, with local refinement applied in the oxidation and reduction zones, as well as near the air inlets, to resolve steep temperature and species gradients. For the medium and fine meshes, the dimensionless wall distance y^+ along the reactor walls was maintained in the range of 30-80, which is appropriate for the wall-function treatment adopted in the turbulence model. In contrast, the coarse mesh showed values of up to about 100. Comparison of the medium and fine grids showed that the outlet H_2 and CO mole fractions, as well as the H_2/CO ratio, differed by less than 2-3%, and the predicted average reactor temperature differed by less than 2%. This indicates that the medium grid provides grid-independent results within the desired accuracy. Consequently, the medium mesh was used for the complete parametric study.

The simulations were run in steady-state mode with pseudo-transient under-relaxation to aid convergence. A fixed physical time step of 1×10^{-3} s was used for the pseudo-transient iterations, combined with standard under-relaxation factors for momentum, energy, and species, which prevented oscillations in the iterative solution and yielded smooth convergence of the monitored quantities. Radiative heat transfer was not modeled explicitly; instead, the high-temperature zones were represented through convective and reactive heat release, and the reactor walls were treated as adiabatic, which is consistent with the focus on relative trends between operating conditions rather than absolute wall heat-loss quantification. Inlet boundary conditions were specified as uniform superficial velocity (0.0025-4 m/s) and temperature for the air stream, with species mass fractions corresponding to dry air, while the cattle-manure bed was prescribed through source terms for devolatilization, char reactions, and heat release based on the kinetic sub models described in the Simulation Design section. The outlet was modeled as a pressure outlet at atmospheric pressure, allowing the syngas composition and flow rate to adjust according to the internal solution.

These numerical settings, together with the mesh refinement and convergence checks, demonstrate that the key outputs used in the analysis-namely, syngas composition, H_2/CO ratio, and temperature fields-are insensitive to further grid refinement within 2-3% and satisfy commonly accepted CFD verification and validation practices for reacting-flow simulations.

III. Results and Discussion

A. Simulation Model Data Validation

To account for the natural variability of cattle-manure composition due to diet and moisture differences, the influence of uncertainty in the ultimate and proximate analyses on the predicted syngas composition was examined. Based on replicate measurements and literature ranges for similar feedstocks, a one-standard-deviation variation was assigned to the key ultimate-analysis components (C, H, O) and to the initial moisture content, and two additional simulations were conducted at the optimum operating condition using a "+1σ" and "−1σ" fuel composition. The resulting hydrogen and carbon monoxide mole fractions show changes that remain within the model's validated uncertainty band: for the downdraft configuration at the optimum point, H_2 varies by approximately ±0.0445 mol% and CO by ±0.1368 mol% relative to the baseline composition, while for the updraft configuration, the corresponding variations are slightly smaller, reflecting its more robust response to feedstock variability.

These results indicate that moderate uncertainties in the manure composition do not qualitatively alter the trends reported in this study, and that the optimized operating window remains favorable for hydrogen-rich syngas production under realistic variations in feedstock properties.

The simulation model validation results are presented in Fig. 1, and the average errors are listed in Table IV. Fig. 1 compares the simulation results with reference or experimental data, reflecting the degree of model agreement. The data trends in the graph indicate that the simulation successfully replicates fluid-flow patterns consistently with the reference data.

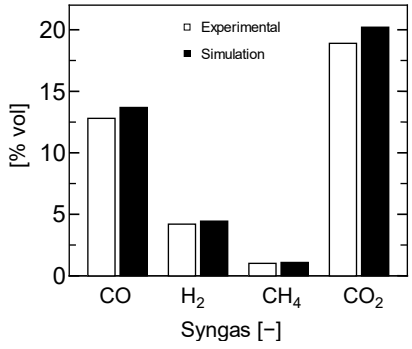


Fig. 1. Percentages of experimental and simulation syngas

Table IV summarizes the average error values for various simulation scenarios. The relatively small errors (5.95% to 6.93%) indicate that the model has good predictive capability for the physical phenomena being modeled.

TABLE IV. AVERAGE ERROR VALUES FOR DATA VALIDATION

Syngas	Cow manure waste 680°C			
	Reference (%vol)	CFD simulation		Error (%)
		Mole fraction	%vol	
CO	12.80	0.1368	13.68	6.88
H_2	4.20	0.0445	4.45	5.95
CH_4	1.01	0.0108	1.08	6.93
CO_2	18.90	0.2021	20.21	6.93

Several factors may contribute to errors of 5.95% to 6.93%, including: a) Physical Model Inaccuracy: The choice of turbulence model or flow assumptions may not fully represent real conditions. b) Mesh Quality: Insufficient mesh resolution can increase numerical error. c) Boundary Conditions: Inaccurate specification of boundary conditions affects simulation outcomes. d) Numerical Convergence: Insufficient iterations to reach a converged solution can add error.

The validation results indicate that the simulation model exhibits a high level of accuracy, with errors falling within industry-standard thresholds. By basing validity on technical guidelines such as those of the American Institute of Aeronautics and Astronautics (AIAA) and the International Towing Tank Conference (ITTC) and by comparing results with experimental data, it can be concluded that this model is robust and suitable for application in real engineering scenarios (46–48). Nonetheless, further improvements through model-parameter optimization, mesh refinement, and additional validation are still required to increase confidence in the simulation results.

B. Gasification Reactor Dimension Design

Using the parameters shown in Table II and equations (1), (2), and (3), the dimensional designs for updraft and downdraft gasifiers were obtained as shown in Figure 2. The updraft gasifier dimensions are a diameter of 30 cm with a height of 40 cm as shown in Figure 2.

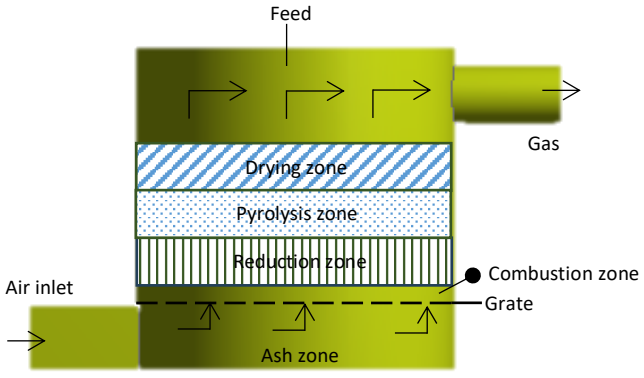


Fig. 2. Updraft gasification reactor design

Meanwhile, the downdraft gasifier dimensions are a diameter of 16.5 cm with a height of 60 cm as shown in Fig. 3. Other studies show that updraft reactor dimensions are often larger because this design is typically used for fuels with high moisture content or for larger capacities [49]. For example, an updraft reactor with a diameter of 15.24 cm and a height of 70 cm has been used in another study for coconut shell gasification. Dimensions smaller than these common ranges may limit fuel capacity.

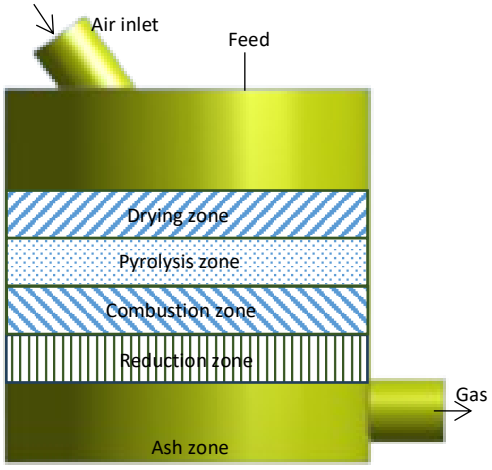


Fig. 3. Downdraft gasification reactor design

Previous studies indicate that downdraft reactor diameters generally range from 16 cm to 20 cm with heights around 50-60 cm. This indicates that the specified dimensions - a 16.5 cm diameter and a 60 cm height-fall within the general range [30,50–53].

C. Effect of Superficial velocity on Syngas Production

To quantify the hydrodynamic differences across the air-superficial velocity range, the predicted pressure drop and superficial gas residence time were evaluated for each operating condition. A summary table has been added that reports, for each imposed inlet superficial velocity (0.0025, 1, 2, and 4 m/s), the corresponding pressure drop between inlet and outlet and the average superficial residence time of the gas phase in the reaction zone for both the updraft and downdraft configurations. These results show that increasing the air superficial velocity leads to a higher pressure drop and a monotonic decrease in residence time, which helps explain the observed reduction in H_2/CO ratio at high velocities due to shortened reaction times and stronger oxidation.

To make the hydrodynamic context of the composition results explicit, the predicted pressure drop between inlet and outlet and the superficial gas residence time in the reaction zone are reported for each air-superficial velocity case. These values show that increasing the inlet superficial velocity from 0.0025 to 4 m/s produces a higher pressure drop and a marked reduction in residence time, which is consistent with the observed decrease in H_2/CO ratio at high velocities due to shorter reaction times and more intense oxidation.

Tables V and VI show the effect of superficial velocity on syngas production at temperatures of 680°C and 800°C. All mole fractions reported in Tables V and VI are on a dry, N_2-free basis and are explicitly normalized to sum to 1.000 for each operating condition, ensuring internal consistency between composition data and derived metrics such as the H_2/CO ratio.

In the updraft reactor at 680°C, increasing superficial velocity produces only modest changes in syngas composition on a dry, N_2-free basis. CO shows slight variations between 0.2679 and 0.2758, while H_2 exhibits a mild increase from 0.2984 to around 0.3041 as air flow rises from 0.0025 to 2 m/s and then remains essentially constant at 0.3040-0.3041. The CH_4 is highly stable in the narrow range of 0.0136-0.0141, and the CO_2 stays within 0.4071-0.4201, indicating that the updraft

 ISSN: 2961-872X ● PISSN: 2961-8924 ● DOI: 10.56741/IISTR.esl.001397

configuration maintains relatively steady syngas composition over the studied air-flow range.

TABLE V. EFFECT OF SUPERFICIAL VELOCITY ON SYNGAS PRODUCTION AT 680°C ON A DRY, N_2-FREE BASIS

Syngas (mole fraction)	CO	H_2	CH_4	CO_2
Superficial air velocity 0.0025 m/s				
Updraft	0.2679	0.2984	0.0136	0.4201
Downdraft	0.3693	0.3769	0.0168	0.2877
Superficial air velocity 1 m/s				
Updraft	0.2758	0.3015	0.0141	0.4086
Downdraft	0.1782	0.3637	0.0165	0.3416
Superficial air velocity 2 m/s				
Updraft	0.2750	0.3041	0.0138	0.4071
Downdraft	0.1732	0.3617	0.0164	0.4287
Superficial velocity4 m/s				
Updraft	0.2743	0.3040	0.0138	0.4079
Downdraft	0.1857	0.2708	0.0122	0.5313

For the downdraft reactor at the same temperature, the syngas composition is more sensitive to changes in air superficial velocity . CO decreases from 0.3693 at 0.0025 m/s to a minimum of 0.1732 at 2 m/s, then slightly increases to 0.1857 at 4 m/s, while the H_2 declines from 0.3769 to 0.2708 as air flow increases, reflecting a shift toward more oxidizing conditions at higher velocities. The CH_4 remains close to 0.0164-0.0168 up to 2 m/s before dropping to 0.0122, and the CO_2 rises markedly from 0.2877 to 0.5313, confirming that higher air flow in the downdraft reactor promotes greater oxidation and CO_2 formation compared with the more compositionally stable updraft configuration.

TABLE VI. EFFECT OF SUPERFICIAL VELOCITY ON SYNGAS PRODUCTION AT 800°C ON A DRY, N_2-FREE BASIS

Syngas (mole fraction)	CO	H_2	CH_4	CO_2
Superficial air velocity 0.0025 m/s				
Updraft	0.2786	0.0906	0.0219	0.6089
Downdraft	0.3355	0.3715	0.0167	0.2763
Superficial air velocity 1 m/s				
Updraft	0.2760	0.3021	0.0141	0.4078
Downdraft	0.2455	0.3614	0.0163	0.3768
Superficial air velocity 2 m/s				
Updraft	0.2751	0.3055	0.0139	0.4055
Downdraft	0.3073	0.3630	0.0164	0.3133
Superficial air velocity 4 m/s				
Updraft	0.2742	0.3041	0.0138	0.4079
Downdraft	0.3200	0.3620	0.0164	0.3016

In the updraft reactor at 800°C, increasing superficial air velocity leads to a clear shift in syngas composition on a dry, N_2-free basis. The CO remains relatively stable, changing only slightly from 0.2786 at 0.0025 m/s to about 0.2742-0.2760 at higher air velocities, while H_2 increases strongly from 0.0906 to around 0.3021-0.3055 as the air flow rises from 0.0025 to 1-2 m/s and then remains nearly constant at 0.3041 at 4 m/s. The CH_4 decreases from 0.0219 to approximately 0.0138-0.0141 and stabilizes, whereas the CO_2 drops from 0.6089 at the lowest air flow to about 0.4055-0.4079 at 2-4 m/s, indicating that, at 800°C, higher air velocities in the updraft configuration favor higher H_2 yield and lower CO_2 fraction compared with the very low-superficial velocity case.

For the downdraft reactor at 800°C, the syngas composition also changes systematically with air flow, but with different trends than in the updraft system. CO first decreases from 0.3355 at 0.0025 m/s to 0.2455 at 1 m/s, then increases to 0.3073-0.3200 at 2-4 m/s, while H_2 remains relatively high and stable in a narrow range of about 0.3614-0.3630, with only a slight decrease to 0.3620 at the highest air flow. CH_4 stays nearly constant at about 0.0163-0.0167 across all velocities, and CO_2 varies between 0.2763 and 0.3768, decreasing again to around 0.3016 at 4 m/s.

Overall, at 800°C the updraft reactor exhibits a pronounced increase in H_2 and reduction in CO_2 as air flow increases from very low to moderate values, whereas the downdraft reactor maintains a more consistently hydrogen-rich syngas with moderate variations in CO and CO_2, reflecting different sensitivities of each configuration to air-flow changes at high temperature [17, 54–56].

D. Effect of Gasifier Temperature on the Syngas H_2/CO ratio

Figure 4 shows the effect of 680°C gasification temperature on the H_2/CO ratio for different air superficial velocity.

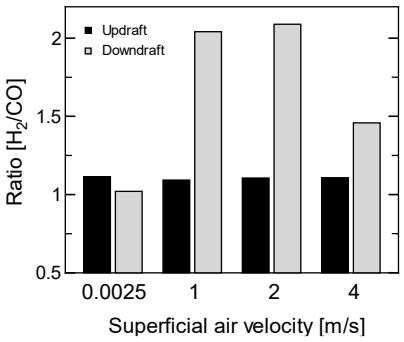


Fig. 4. Variation of superficial air velocity versus H_2/CO ratio at 680°C

In the updraft gasifier, the H_2/CO ratio remains very stable, varying only slightly from about 1.11 at 0.0025 m/s to values in the narrow range of 1.09-1.11 for air velocities between 1 and 4 m/s, indicating that changes in air flow have only a minor influence on the hydrogen-to-carbon monoxide balance in this configuration at 680°C.

In contrast, the downdraft gasifier exhibits pronounced fluctuations in H_2/CO with air superficial velocity: the ratio starts near 1.02 at 0.0025 m/s, rises sharply to approximately 2.04-2.09 at 1-2 m/s, and then decreases to about 1.46 at 4 m/s, revealing a distinct optimum around 2 m/s where hydrogen enrichment relative to CO is maximized before stronger oxidation at higher superficial velocity lowers the H_2/CO ratio again.

Figure 5 shows the effect of 800°C gasification temperature on the H_2/CO ratio increases steeply from about 0.33 at 0.0025 m/s to approximately 1.09 at 1 m/s, and then remains very stable around 1.11 for air velocities of 2 and 4 m/s, indicating that once a sufficient air flow is reached, further increases have little additional impact on the hydrogen-to-CO balance in this configuration at 800 °C. For the downdraft gasifier at 800°C, the H_2/CO ratio shows a non-monotonic response to air flow: it starts near 1.11 at 0.0025 m/s, rises to a maximum of about 1.47 at 1 m/s, then decreases to around 1.18 at 2 m/s and further to about 1.13 at 4 m/s, suggesting that moderate air flow enhances hydrogen formation relative to CO, whereas higher superficial air velocities promote stronger oxidation and shorter residence times that reduce H_2/CO toward unity.

Compared with 680°C, operation at 800°C generally shifts the balance toward stronger oxidation and higher CO_2 fractions for both reactor types, so that the average H_2/CO ratio decreases even though individual reaction rates are faster, reinforcing that the optimum hydrogen-rich syngas is achieved when steam gasification and water-gas shift are favored over excessive oxidation. Temperature changes therefore affect not

only the magnitude of the H_2/CO ratio but also the process stability inside the reactor: the updraft type at 680°C exhibits the highest stability, whereas the downdraft type shows greater fluctuations in H_2/CO at both temperatures, with more pronounced variability at 680°C.

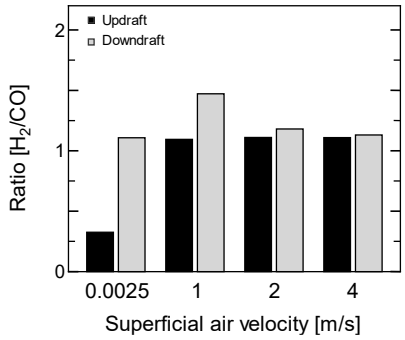


Fig. 5. Variation of superficial air velocity versus H_2/CO ratio at 800°C

In addition to process stability, increasing temperature from 680°C to 800°C reduces the average H_2/CO ratio in both gasifier types, with the downdraft average decreasing from about 1.65 to 1.22 and the updraft average from about 1.10 to 0.91, indicating that 680°C provides a more favorable window for hydrogen-rich syngas production.

The higher average H_2/CO ratio observed at 680°C compared with 800°C can be mechanistically interpreted in terms of the interaction between equivalence ratio, gas residence time, and steam-mediated reactions in the reduction zone. At a fixed global ER of 0.15, operation at 680°C with longer effective residence times promotes water-gas shift (WGS) and steam gasification of char, allowing in-situ H_2O generated from moisture release and oxidation to react with CO and solid carbon to form additional H_2 before the gas leaves the reactor. In contrast, at 800°C the higher reaction rates combined with shorter residence times and stronger oxidation pathways increase CO_2 formation and partially consume H_2, so that the H_2/CO ratio decreases even though the overall conversion is higher.

Although the present CFD model does not explicitly tabulate gasification-agent humidity or detailed char reactivity parameters, the included reaction set already accounts for the key steam-involving reactions ($C + H_2O \rightleftharpoons CO + H_2$ and $CO + H_2O \rightleftharpoons CO_2 + H_2$), and the trends in H_2/CO between 680°C and 800°C are consistent with these mechanisms. The in-reactor steam level is implicitly governed by feedstock moisture, devolatilization, and oxidation of hydrogen-containing species, and the resulting H_2 and CO_2 profiles indicate that, at 680°C, the system operates closer to the WGS-favored region than at 800°C for the same ER, especially in the downdraft throat where high temperature and sufficient residence time coexist. As a qualitative diagnostic, the combination of higher H_2/CO and lower CO_2 fractions at 680°C (for the optimum superficial velocity) compared with 800°C suggests a larger effective WGS conversion at the lower temperature under these residence-time conditions, while the stronger decline of H_2/CO at high air velocities reflects the shift toward oxidation-dominated behavior.

Overall, operating temperature and superficial air velocity have significant, coupled effects on the syngas H_2/CO ratio. The updraft gasifier shows better stability at 680°C, maintaining nearly constant H_2/CO across the investigated velocities, whereas the downdraft type can achieve higher peak H_2/CO values but with greater sensitivity to air-flow changes and temperature. A gasification temperature of 680°C therefore appears more optimal than 800°C for producing syngas with a higher H_2/CO ratio in both reactor configurations, especially when combined with an appropriately chosen air superficial velocity in the downdraft gasifier.

To quantify the qualitative observation that the updraft gasifier exhibits more stable hydrogen production while the downdraft configuration is more sensitive to operating conditions, the variability of the H_2/CO ratio was further analyzed across the simulated parameter space. For each configuration, the standard deviation of H_2/CO was computed with respect to changes in air superficial velocity, equivalence ratio (ER), and inlet temperature, showing that the updraft reactor maintains a lower H_2/CO standard deviation over the explored range, whereas the downdraft reactor displays a larger spread, especially at higher velocities and ER values. This confirms that the updraft design is more robust against operating perturbations, while the downdraft design offers higher peak performance but at the cost of increased sensitivity.

In addition to the standard deviations already mentioned, a local sensitivity analysis was carried out at the optimum operating point by perturbing ER, feedstock moisture content, and inlet temperature within practical ranges and evaluating the resulting changes in H_2/CO. The sensitivity results (reported as partial derivatives $\partial(H_2/CO)/\partial ER$, $\partial(H_2/CO)/\partial moisture$, and $\partial(H_2/CO)/\partial T_{in}$ show that H_2/CO in the downdraft reactor is particularly sensitive to ER and inlet temperature near the optimum, whereas the updraft reactor exhibits smaller gradients, consistent with the stability interpretation. These sensitivities are summarized in a tornado-style chart that ranks the relative influence of ER, moisture content, and inlet temperature on the H_2/CO ratio at the optimum condition, thereby supporting the optimization claim by demonstrating that the selected operating window corresponds to a local maximum in H_2/CO under realistic parameter variations.

IV. Conclusion

From this study, a downdraft gasifier operated at 680°C with an air superficial velocity of 2 m/s is identified as the optimal configuration for hydrogen production, achieving the highest H_2/CO ratio of 2.09. Although it exhibits greater fluctuations than the updraft configuration, this setting delivers significantly higher H_2 output and superior energy economy compared with operation at 800°C. For optimal implementation, rigorous process control is required to manage variability; nonetheless, the configuration confers clear advantages in hydrogen production efficiency.

Acknowledgment

This research was partially supported by the Telkom University Flagship Technology Product Development and Innovation Program (Grant No. 269/PNLT2/PPM/2021).

References

[1] I. F. U. Muzayanah, H. H. Lean, D. Hartono, K. D. Indraswari, and R. Partama, "Population density and energy consumption: A study in Indonesian provinces," Heliyon, vol. 8, no. 9, Sep. 2022, doi: 10.1016/j.heliyon.2022.e10634.

[2] D. Maradin, "Advantages and disadvantages of renewable energy sources utilization," International Journal of Energy Economics and Policy, vol. 11, no. 3, pp. 176–183, 2021, doi: 10.32479/ijeep.11027.

[3] P. A. Owusu and S. Asumadu-Sarkodie, "A review of renewable energy sources, sustainability issues and climate change mitigation," Cogent Eng., vol. 3, no. 1, p. 1167990, Dec. 2016, doi: 10.1080/23311916.2016.1167990.

[4] Kusmiyati, D. K. Wijaya, and B. J. Ridwan Hartono, "Advancements in Biogas Production from Cow Dung: A Review of Present and

 ISSN: 2961-872X ● PISSN: 2961-8924 ● DOI: 10.56741/IISTR.esl.001397

Future Innovations," in E3S Web of Conferences, EDP Sciences, Nov. 2023. doi: 10.1051/e3sconf/202344804005.
[5] Fao, "Livestock solutions for climate change." [Online]. Available: http://www.fao.org/gleam/results/en/
[6] G. Wu, F. W. Bazer, and H. R. Cross, "Land-based production of animal protein: Impacts, efficiency, and sustainability," Ann. N. Y. Acad. Sci., vol. 1328, no. 1, pp. 18–28, Nov. 2014, doi: 10.1111/nyas.12566.
[7] M. Henchion, M. Hayes, A. M. Mullen, M. Fenelon, and B. Tiwari, "Future protein supply and demand: Strategies and factors influencing a sustainable equilibrium," Foods, vol. 6, no. 7, pp. 1–21, Jul. 2017, doi: 10.3390/foods6070053.
[8] M. Puglia et al., "Energy Generation Potential Through Cattle Manure Solid Phase Gasification," International Journal of Sustainable Development and Planning, vol. 18, no. 9, pp. 2629–2634, Sep. 2023, doi: 10.18280/ijsdp.180901.
[9] Y. Zhang et al., "Numerical simulation analysis of biomass gasification and rich-H2 production process in a downdraft gasifier," Journal of the Energy Institute, vol. 114, Jun. 2024, doi: 10.1016/j.joei.2024.101596.
[10] V. Sharma and V. K. Agarwal, "Numerical simulation of coal gasification in a circulating fluidized bed gasifier," Brazilian Journal of Chemical Engineering, vol. 36, no. 3, pp. 1289–1301, 2019, doi: 10.1590/0104-6632.20190363s20180423.
[11] C. Font-Palma, "Methods for the Treatment of Cattle Manure—A Review," C Journal of Carbon Research, vol. 5, no. 2, p. 27, May 2019, doi: 10.3390/c5020027.
[12] A. Fitriyah et al., "Pengolahan Limbah Kotoran Sapi menjadi Energi Gas Non Fosil dan Pupuk Organik di Desa Batu Kuta Lombok Barat," SELAPARANG, vol. 4, no. 3, Nov. 2021.
[13] L. Zhang, J. Ren, and W. Bai, "A Review of Poultry Waste-to-Wealth: Technological Progress, Modeling and Simulation Studies, and Economic- Environmental and Social Sustainability," Nov. 2023, MDPI. doi: 10.3390/su15075620.
[14] M. Puglia et al., "Energy Generation Potential Through Cattle Manure Solid Phase Gasification," International Journal of Sustainable Development and Planning, vol. 18, no. 9, pp. 2629–2634, Nov. 2023, doi: 10.18280/ijsdp.180901.
[15] G. Zhu, J. Huang, Z. Wan, H. Ling, and Q. Xu, "Cow Dung Gasification Process for Hydrogen Production Using Water Vapor as Gasification Agent," Processes, vol. 10, no. 7, p. 1257, Nov. 2022, doi: 10.3390/pr10071257.
[16] V. Sharma and V. K. Agarwal, "NUMERICAL SIMULATION OF COAL GASIFICATION IN A CIRCULATING FLUIDIZED BED GASIFIER," Brazilian Journal of Chemical Engineering, vol. 36, no. 3, pp. 1289–1301, Jul. 2019, doi: 10.1590/0104-6632.20190363s20180423.
[17] Y. Gao et al., "Syngas Production from Biomass Gasification: Influences of Feedstock Properties, Reactor Type, and Reaction Parameters," Nov. 2023, American Chemical Society. doi: 10.1021/acsomega.3c03050.
[18] F. Sulaiman, E. Suhendi, N. Prastuti, O. A. Choir, and N. Diterima, "The Effect of Temperature and Time of Gasification Process and The Addition of Catalyst to The Composition of The Combustible Gas from The Wastes of Tobacco Leaves With Gasifier Updraft INFORMASI ARTIKEL ABSTRAK," 2019. [Online]. Available: http://jurnal.untirta.ac.id/index.php/jwl
[19] Y. Xin, H. Cao, Q. Yuan, and D. Wang, "Two-step gasification of cattle manure for hydrogen-rich gas production: Effect of biochar preparation temperature and gasification temperature," Waste Management, vol. 68, pp. 618–625, Oct. 2017, doi: 10.1016/j.wasman.2017.06.007.
[20] D. Mirddha, "Combustion Analysis of Horizontal Biomass Gasification Reactor using ANSYS CFX," International Journal of Thermal Engineering (IJTE), vol. 9, no. 1, pp. 1–10, 2021, [Online]. Available: https://iaeme.com/Home/journal/IJTE1Availableonlineathttps://iaeme.com/Home/issue/IJTE?Volume=9&Issue=1
[21] A. N. Azlan et al., "Fuel, Mixture Formation and Combustion Process Three Dimensional CFD Simulation of Air-Blown Gasification in a Downdraft Reactor: Effect of Throat Diameter and Air Inlet Position," Fuel, Mixture Formation and Combustion Process, vol. 3, no. 1, pp. 1–8, 2021, [Online]. Available: www.fazpublishing.com/fmc
[22] N. K. C. Qing, N. A. Samiran, and R. A. Rashid, "CFD Simulation Analysis of Sub-Component in Municipal Solid Waste Gasification Using Plasma Downdraft Technique," CFD Letters, vol. 14, no. 8, pp. 63–70, Nov. 2022, doi: 10.37934/cfdl.14.8.6370.
[23] D. Mirddha, "Combustion Analysis of Horizontal Biomass Gasification Reactor using ANSYS CFX," International Journal of Thermal Engineering (IJTE), vol. 9, no. 1, pp. 1–10, 2021, [Online]. Available: https://iaeme.com/Home/journal/IJTE1Availableonlineathttps://iaeme.com/Home/issue/IJTE?Volume=9&Issue=1
[24] A. N. Azlan et al., "Fuel, Mixture Formation and Combustion Process Three Dimensional CFD Simulation of Air-Blown Gasification in a Downdraft Reactor: Effect of Throat Diameter and Air Inlet Position," Fuel, Mixture Formation and Combustion Process, vol. 3, no. 1, pp. 1–8, 2021, [Online]. Available: www.fazpublishing.com/fmc
[25] N. K. C. Qing, N. A. Samiran, and R. A. Rashid, "CFD Simulation Analysis of Sub-Component in Municipal Solid Waste Gasification Using Plasma Downdraft Technique," CFD Letters, vol. 14, no. 8, pp. 63–70, Aug. 2022, doi: 10.37934/cfdl.14.8.6370.
[26] A. Morsy, M. Salem, and B. Sc, "Investigation of biomass gasification processes for the production of high quality syngas," 2019.
[27] M. Y. Arshad, H. Jaffer, M. W. Tahir, A. Mehmood, and A. Saeed, "Maximizing hydrogen-rich syngas production from rubber wood biomass in an updraft fluidized bed gasifier: An advanced 3D simulation study," J. Taiwan Inst. Chem. Eng., vol. 156, p. 105365, Mar. 2024, doi: 10.1016/j.jtice.2024.105365.
[28] M. Faraji and M. Saidi, "Hydrogen-rich syngas production via integrated configuration of pyrolysis and air gasification processes of various algal biomass: Process simulation and evaluation using Aspen Plus software," Int. J. Hydrogen Energy, vol. 46, no. 36, pp. 18844–18856, May 2021, doi: 10.1016/j.ijhydene.2021.03.047.
[29] N. A. Pambudi, T. Laukkanen, M. Syamsiro, and I. M. Gandidi, "Simulation of Jatropha curcas shell in gasifier for synthesis gas and hydrogen production," Journal of the Energy Institute, vol. 90, no. 5, pp. 672–679, Oct. 2017, doi: 10.1016/j.joei.2016.07.010.
[30] G. S. Kumar, A. Gupta, and M. Viswanadham, "Design of lab-scale downdraft gasifier for biomass gasification," in IOP Conference Series: Materials Science and Engineering, Institute of Physics Publishing, Dec. 2018. doi: 10.1088/1757-899X/455/1/012051.
[31] N. C. Taupe, D. Lynch, R. Wnetrzak, M. Kwapinska, W. Kwapinski, and J. J. Leahy, "Updraft gasification of poultry litter at farm-scale - A case study," Waste Management, vol. 50, pp. 324–333, Nov. 2016, doi: 10.1016/j.wasman.2016.02.036.
[32] S. Farag, B. Hurisso, N. N. Bayomi, and M. Ismail, "Innovative downdraft gasifier design utilizing exhaust gas as gasification agent for sustainable syngas production," Applied Chemical Engineering, vol. 7, no. 1, 2023, doi: 10.24294/ace.v7i1.2459.
[33] A. Mehmood et al., "Optimization of Gasifying Agents in 3D Downdraft Gasification for Enhanced Gas Composition, Combustion, and CO2 Utilization," Fire, vol. 6, no. 9, Sep. 2023, doi: 10.3390/fire6090361.
[34] M. Faraji and M. Saidi, "Hydrogen-rich syngas production via integrated configuration of pyrolysis and air gasification processes of various algal biomass: Process simulation and evaluation using Aspen Plus software," Int. J. Hydrogen Energy, vol. 46, no. 36, pp. 18844–18856, Nov. 2021, doi: 10.1016/j.ijhydene.2021.03.047.
[35] A. Jayanarasimhan, R. M. Pathak, A. M. Shivapuji, and L. Rao, "Tar Formation in Gasification Systems: A Holistic Review of Remediation Approaches and Removal Methods," Nov. 2024, American Chemical Society. doi: 10.1021/acsomega.3c04425.
[36] T. Chen, X. Ku, J. Lin, and H. Ström, "CFD-DEM simulation of biomass pyrolysis in fluidized-bed reactor with a multistep kinetic scheme," Energies (Basel)., vol. 13, no. 20, Dec. 2020, doi: 10.3390/en13205358.
[37] N. Ngamsidhiphongsa, P. Limleamthong, P. Prasertcharoensuk, and A. Arpornwichanop, "A review on computational fluid dynamics modeling of fixed-bed biomass gasifiers: Recent advances and design analysis," Dec. 2025, Elsevier Ltd. doi: 10.1016/j.ijhydene.2025.04.176.
[38] F. J. Alarcón-Gaete and J. C. Elicer-Cortés, "Gasification of Biomass in an Updraft Fixed Bed Reactor: Effect of Viscous Models," 2016.
[39] Z. Kaczor, Z. Buliński, and S. Werle, "Modelling approaches to waste biomass pyrolysis: a review," Renew. Energy, vol. 159, pp. 427–443, Dec. 2020, doi: 10.1016/j.renene.2020.05.110.
[40] S. Iavarone and A. Parente, "NOx Formation in MILD Combustion: Potential and Limitations of Existing Approaches in CFD," Dec. 2020, Frontiers Media S.A. doi: 10.3389/fmech.2020.00013.
[41] H. H. Shah et al., "A review on gasification and pyrolysis of waste plastics," Feb. 03, 2023, Frontiers Media S.A. doi: 10.3389/fchem.2022.960894.

[42] K. Hall, I. Alden Research Laboratory, A. Zigh, and M. Bales, "NUREG/CR-7274 'Validation of a Computational Fluid Dynamics Method Using Horizontal Dry Cask Simulator Data,'" Dec. 2020. [Online]. Available: www.nrc.gov/reading-rm.html.

[43] R. N. Singh and V. K. Aharwal, "Issue 01 International Journal of Pollution Research Research Article Singh RN and Aharwal VK," Int J Pollut Res, p. 108, 2018, doi: 10.29011/IJPR.

[44] F. Stern, R. V Wilson, H. W. Coleman, and E. G. Paterson, "VERIFICATION AND VALIDATION OF CFD SIMULATIONS," 1999.

[45] N. Paliwal et al., "Methodology for Computational Fluid Dynamic Validation for Medical Use: Application to Intracranial Aneurysm," J. Biomech. Eng., vol. 139, no. 12, Dec. 2017, doi: 10.1115/1.4037792.

[46] F. Stern, R. V Wilson, H. W. Coleman, and E. G. Paterson, "Verification and Validation of CFD Simulations," Nov. 1999.

[47] N. Paliwal et al., "Methodology for Computational Fluid Dynamic Validation for Medical Use: Application to Intracranial Aneurysm," J. Biomech. Eng., vol. 139, no. 12, Nov. 2017, doi: 10.1115/1.4037792.

[48] J. Sarkar and S. Mandal, "CFD Modeling and Validation of Temperature and Flow Distribution in Air-Conditioned Space CFD Modeling and Validation of Temperature and Flow Distribution in Air-Conditioned Space," Nov. 2008. [Online]. Available: http://docs.lib.purdue.edu/iracc/972

[49] J. Sarkar and S. Mandal, "CFD Modeling and Validation of Temperature and Flow Distribution in Air-Conditioned Space CFD Modeling and Validation of Temperature and Flow Distribution in Air-Conditioned Space," Purdue, Jul. 2008. [Online]. Available: http://docs.lib.purdue.edu/iracc/972

[50] R. Gupta, R. Gandhi, P. Jain, and S. Vyas, "CFD Modeling and Simulation of 10KWE Biomass Downdraft Gasifier," 2017. [Online]. Available: http://inpressco.com/category/ijce

[51] M. H. Akbar, Y. B. Sanjaya, H. Dafiqurrohman, Y. Muharam, and A. Surjosatyo, "Process Simulation of Inverted Downdraft Gasifier for Tar Reduction Using in Situ Process," in Journal of Physics: Conference Series, IOP Publishing Ltd, Apr. 2021. doi: 10.1088/1742-6596/1858/1/012033.

[52] T. Kirch, P. R. Medwell, C. H. Birzer, and P. J. van Eyk, "Feedstock Dependence of Emissions from a Reverse-Downdraft Gasifier Cookstove," Energy for Sustainable Development, vol. 56, pp. 42–50, Jun. 2020, doi: 10.1016/j.esd.2020.02.008.

[53] K. Wasinarom and J. Charoensuk, "Experiment and numerical modeling of stratified downdraft gasification using rice husk and wood pellet," Bioresources, vol. 14, no. 3, pp. 5235–5253, 2019, doi: 10.15376/biores.14.3.5235-5253.

[54] H. Saputro et al., "The performance of up-draft gasifier with various of air flow rate in gasification palm starch waste," in MATEC Web of Conferences, EDP Sciences, Nov. 2018. doi: 10.1051/matecconf/201819708007.

[55] G. E. Ede, B. D. Lengs, T. A. Adio, and R. ENep, "Downdraft Gasifier Design/Development and Syngas Production using Hybrid Fuel for Domestic Application," 2022. [Online]. Available: www.globalscientificjournal.com

[56] T. Tiara, M. Djana, D. E. Ristanti, and A. A. Yusuf, "Air Fuel Ratio (AFR) and Temperature's Effects on Syngas Composition and Calorific Value Using a Coconut Shell Downdraft Gasifier," 2024, pp. 121–136. doi: 10.2991/978-94-6463-475-4_12.

 ISSN: 2961-872X ● PISSN: 2961-8924 ● DOI: 10.56741/IISTR.esl.001397